RESEARCH ARTICLE

NANO · MICRO small
www.small-journal.com

Inverse Opal Torus-Shaped Photonic Microobjects with Superior Stimulus-Responsive Properties to Their Spherical Equivalents

Xiaoyang Du, Shuchen Zhang, Junqi Zhou, Hongxiang Chi, ZheJia Sheng, Yuandu Hu, Chao Shang, Tao Wang,* Guang Chen, and Zhenzhong Yang**

Because of their many uses and simplicity of manufacture, colloidal photonic microobjects made from droplet templates have been the subject of extensive research. Owing to the low interfacial energy, the majority are spherical, however nonspherical forms, such as torus-shaped photonic microobjects (TSPMs) have also been seen. Although there have been reports of TSPMs based on various colloidal building blocks, their usual lack of stimulus-responsive qualities restricts their potential uses. In this work, hydrogel-based inverse opal TSPMs (IO-TSPMs) that are sensitive to alcohol and pH are created. IO-TSPMs that react more quickly than spherical ones are produced by first creating opal-structured TSPMs, then infiltrating monomers, polymerizing under UV light, and etching, to visibly illustrate the difference. Unlike spherical structures, which only provide unidirectional stimulus propagation, torus structures allow stimulation to bidirectionally propagate from both the inner and outer borders. Potential applications for these IO-TSPMs include biomimetic materials, quick diagnostic and inspection tools, and building blocks for innovative patterns.

1. Introduction

Colloidal photonic microobjects are widely used in a variety of industries, including coating, pigments to sensors, and anticounterfeiting structures.[1] Since spherical droplets have the lowest interfacial energy, photonic microobjects that are templated from them are often spherical in shape.[2] Interestingly, nonspherical microobjects may be more common in some places.[3] To adapt to their surroundings, numerous microbes, for instance, have developed nonspherical forms over extended periods of time. The feathers of peacocks and the epidermis of chameleons are examples of living things with structural colors that have nonspherical body forms.[4] It has been observed that the reflection intensity of plate-like photonic microobjects, which are made from the assembly of polystyrene colloidal particles (CPs) is higher than that of photonic microspheres (PMSs).[5] By adjusting different parameters, researchers have created colloidal photonic microobjects with a range of shapes, including rod-like, bowl-like, and micro ellipsoidal to torus-shaped (TS), by playing with different parameters.[6–8] Among these, TSPMs are especially intriguing since the hole at the core of the microobject can provide special characteristics that could change its characteristics.[9,10] However, all of the few publications on TSPMs from spherical droplet templates have an opal structure and lack stimulus-responsive qualities,[11] which are essential for photonic microobjects used

X. Du, S. Zhang, J. Zhou, H. Chi, Z. Sheng, Y. Hu
Department of Materials Science and Engineering
School of Physical Science and Engineering
Beijing Jiaotong University
Beijing 100044, China
E-mail: huyd@bjtu.edu.cn

Y. Hu
Hubei Provincial Key Laboratory of Green Materials for Light Industry
Hubei University of Technology
Wuhan 430068, China

Y. Hu
Guangdong Provincial Key Laboratory of Technique and Equipment for Macromolecular
Advanced Manufacturing
South China University of Technology
Guangzhou 510641, China

The ORCID identification number(s) for the author(s) of this article can be found under https://doi.org/10.1002/smll.202412117

DOI: 10.1002/smll.202412117

Y. Hu, Z. Yang
Key Laboratory of Advanced Materials of Ministry of Education
Department of Chemical Engineering Tsinghua University
Beijing 100084, China
E-mail: yangzhenzhong@tsinghua.edu.cn

C. Shang
Department of Physics
School of Physical Science and Engineering
Beijing Jiaotong University
Beijing 100044, China

T. Wang
Metals and Chemistry Research Institute
China Academy of Railway Sciences Corporation Limited
Beijing 100081, China
E-mail: 027wangtao@163.com

G. Chen
Department of Advanced Manufacturing and Robotics
College of Engineering
Peking University
Beijing 100871, China

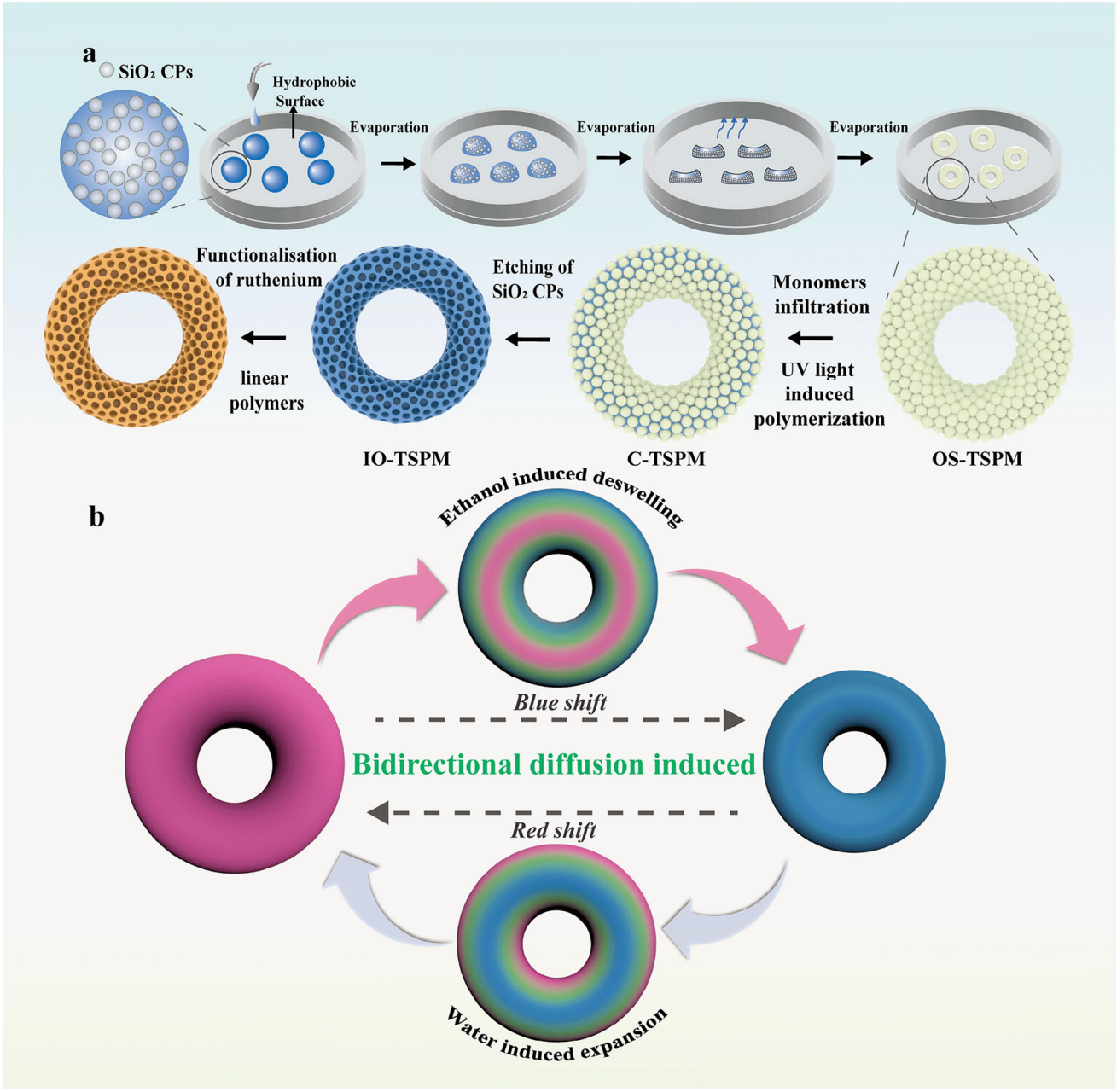

Scheme 1. a) Schematic illustrating the preparation and construction of IO-TSPMs. b) Schematic diagram of bidirectional induced diffusion of IO-TSPM.

for anticounterfeiting, camouflage, and sensing etc.[12] Furthermore, it has been noted that TS microobjects have shorter diffusion paths than spherical ones.[13] To date, the development and analysis of stimulus-responsive TSPMs have not yet been thoroughly examined. More significantly, no concrete and observable proof that TS photonic microobjects are better than spherical microobjects has been offered.

We present the construction and property research of TSPMs with an inverse opal structure in light of this. Spherical droplets with an aqueous dispersion of monodispersed SiO_2 CPs were created and gathered on a hydrophobic surface in order to create the microobjects. As the solvent evaporated, the droplets transformed into a variety of shaped colloidal photonic microobjects. Because of the synergistic effects of capillary flow and other physical phenomena during the procedure, TSPMs can be generated by varying the experimental settings.[14] SiO_2 CPs-hydrogel composite TSPMs (C-TSPMs) were produced by UV light-induced polymerization following the infiltration of the voids among the SiO_2 CPs of the TSPMs with an aqueous solution of monomers (acrylamide, acrylic acid) and a crosslinker (N, N'-methylenebisacrylamide). Wet etching was used to further transform the C-TSPMs into IO-TSPMs (**Scheme 1a**). The IO-TSPMs exhibit alcohol-/pH-induced alterations in optical phenomena because polyacrylamide (pAAm)-based skeletons are

alcohol- and pH-responsive. Additionally, through intermolecular interactions, ruthenium compounds were added to the IO-TSPMs' skeleton giving the microobjects their fluorescence. From a visualization standpoint, the IO-TSPMs were demonstrated to have faster response speeds than PMSs, and the mechanism was suggested (Scheme 1b). The faster response speeds were exhibited both in terms of water absorption-induced swelling from a dehydrated state and alcohol-induced deswelling from a hydrated state. The IO-TSPMs could be used in fields like microsensors and sophisticated photonic microdevices. This approach can be used to create new structures out of a variety of different materials.

2. Results and Discussion

Scheme 1a depicts the construction and preparation of IO-TSPMs, while Scheme S1 (Supporting Information) depicts IO-PMSs. In essence, spherical droplets of an aqueous dispersion of monodispersed SiO_2 CPs were prepared and collected on hydrophobic surfaces (Figures S1and S2, Supporting Information). The initial droplets' sizes were mainly manipulated by varying the inner diameter of the injection tube (details are shown in Table S1, Supporting Information). Following evaporation, the SiO_2 CPs spontaneously assembled into a variety of colloid-based superstructures (Figures S3–S7, Supporting Information).[15]

By utilizing the complementary effects of capillary flow and multiple other physical phenomena, including Brownian motion, sedimentation, etc., colloid-based TS superstructures can be produced.[7,16] OS-TSPMs can be obtained through the manipulation of several factors (Figures S3–S6, Supporting Information). Photographs taken from the top and side showed that the droplet's evolution took ≈10 min to complete (Figures S8–S10, Supporting Information). A neck-like structure among SiO_2 CPs may be introduced by calcination at 750 °C, improving the mechanical properties of the OS-TSPMs.[17] A solution of AAm, AAc, and cross-linker BIS was then used to infiltrate the spaces between SiO_2 CPs. The UV light-induced curing process transformed the OS-TSPMs into C-TSPMs, which were further turned into IO-TSPMs by etching the SiO_2 CPs. The IO-TSPMs demonstrated reversible stimulus-responsive properties, as illustrated in Scheme 1b.

The sizes of the SiO_2 CPs can be used to adjust the structural colors of the OS-TSPMs. The statistical plots of SiO_2 CPs with varying average diameters and the related TEM images are displayed in Figure S11a–c (Supporting Information). The matching OS-TSPMs made from the assembly of the SiO_2 CP are displayed in **Figure 1**a–c. For instance, OS-TSPMs with blue, green, and red hues are formed by SiO_2 CPs with average diameters of 204, 246, and 300 nm, respectively. Accordingly, 467, 521, and 624 nm were the maximum reflection spectra peaks of the OS-TSPMs, respectively (Figure S12, Supporting Information). The Bragg equation's basic form can be used to explain these values, which were in good harmony with the structural colors:

$$n\lambda = 2d\sin\theta \quad (1)$$

Where n, d, and θ stand for the diffraction order, the lattice spacing, and the incident light angle, respectively. In our scenario, n is assumed to be 1 (first-order diffraction), and θ is 90°. The diameter of the SiO_2 CPs is correlated with d. As seen in Figure 1d,e, the microobjects had a curved top and a flat bottom surface.

Using the green OS-TSPM as an example, a striking green structural color is visible on both the microobject's curved surface (Figure 1b) and flat surface (Figure 1f), but with a somewhat distinct photonic phenomenon. In Figure 1g, the peaks of the curved and flat surfaces' reflection spectra are situated at 522 and 516 nm, respectively. Furthermore, the peak on the flat surface was narrower and more intense than the peak on the curved surface. Because the light scattering effect on flat surfaces was smaller and the direction of the reflected light was more focused, there was a tiny difference between the flat and curved surfaces. As a result, the reflection peak from the flat surface tended to be sharper and more intense. In contrast, the curved surface caused the incident light to be reflected in a different direction and the direction of the reflected light to be scattered, resulting in a weaker and wider reflection peak.[18] Figure 1h–l are OM images of various modes of the green microobject after calcining. In Figure 1m, the reflection spectrum peak of the microobject after calcining was located at 495 nm, exhibiting a slight blue shift when compared with the value of 520 nm prior to calcining (also shown in Figure S13 (Supporting Information) for initial blue and red TSPMs). This blue shift was caused by the tighter packing and the formation of silicon-oxygen bonds (Si—O—Si) among the SiO_2 CPs during the calcining process.[19] The microscopic distinction between the flat and curved surfaces was also discovered by additional SEM photography of the microobject. The SEM pictures of the microobject's curved and flat surfaces are shown in Figure 1n–s. SiO_2 CPs showed outward packing structures at the outer edge(o) of the curved surface and inward packing structures at the inner edge(p), respectively. Following self-assembly, the SiO_2 CPs evidently displayed a flawless hexagonal structure in the center of the microobject's flat surface(s) and curved surface(q).

The monomers filled OS-TSPMs were converted into SiO_2 CPs-hydrogel C-TSPMs by applying UV light irradiation, and then wet etching was used to further convert them into IO-TSPMs. As an example, we used the green OS-TSPMs. A C-TSPM's transition to an IO-TSPM is depicted in **Figure 2**a–f (also shown in Figure S14, Supporting Information). After the C-TSPM was converted into an IO-TSPM, the maximum reflection wavelength moved from 537 to 499 nm, according to the matching reflection spectra in Figure 2h (also shown in Figure S15 (Supporting Information) for C-TSPMs with initial blue and red colors).

According to Bragg's equation, the interaction between variations in lattice spacing (d_{111}) and the effective refractive index (n_{eff}) can account for the shift in maximum reflection wavelength:

$$\lambda_{111} = 2d_{111}n_{eff} \quad (2)$$

Before etching, the polymer skeleton was confined within the close-packed SiO_2 CPs of the TSPM, which meant that the close-packed SiO_2 CPs dominated photonic properties. However, after etching, this constraint was removed, resulting in a drop in the refractive index n from ∼1.41 (the Supporting Information shows the calculation details for the SiO_2 CPs-hydrogel C-TSPM in) to ∼1.33 (the refractive index of the hydrogel network after

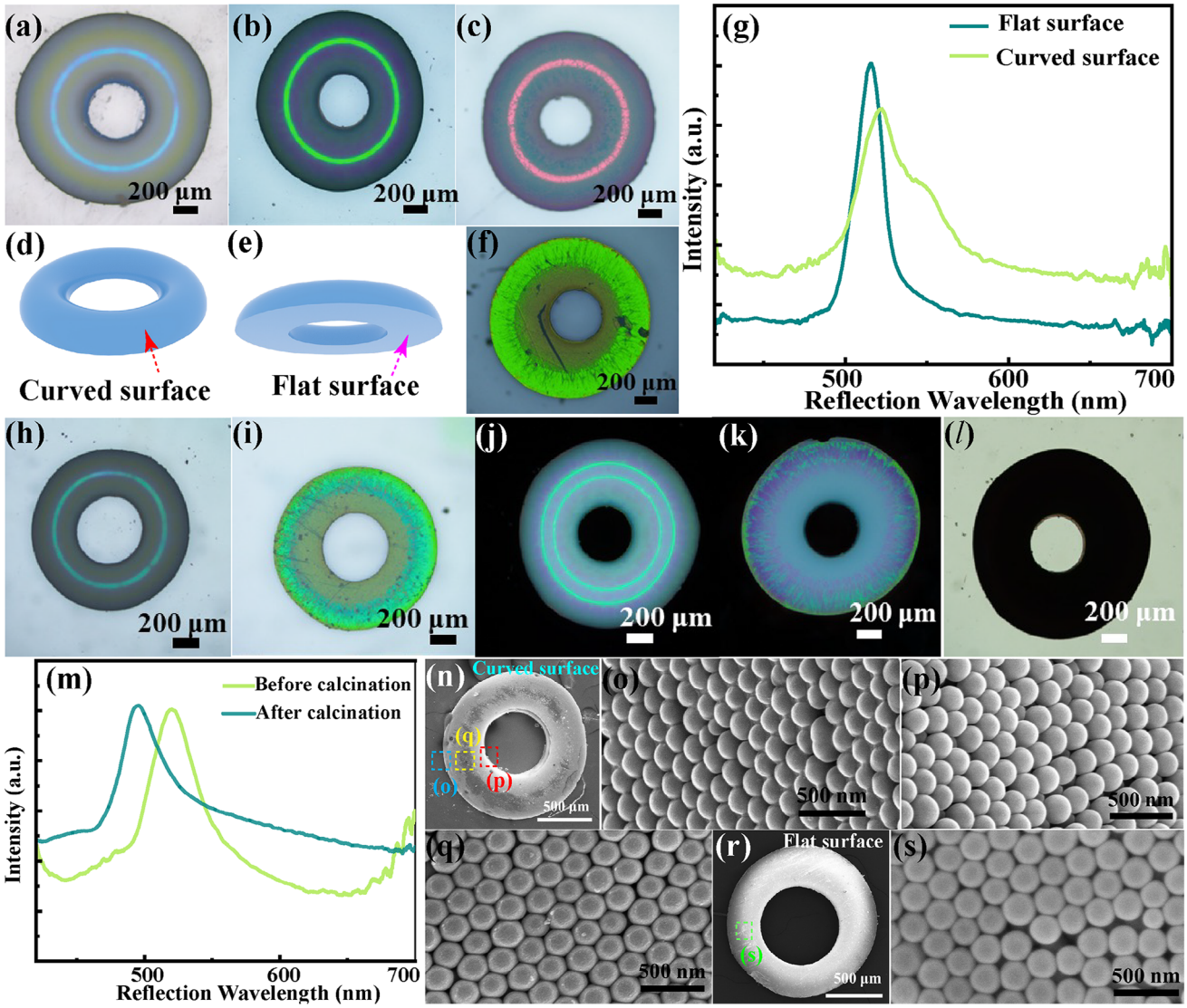

Figure 1. a–c) Optical microscopy (OM) images of OS-TSPMs with different colors. d,e) Cartoon schematic diagrams of the OS-TSPM's curved surface d) and flat surface e). f) the flat surface of the OS-TSPM before calcining under a bright field (reflection mode). g) Reflectance spectra of the OS-TSPM's curved surface and flat surface. h–*l*) OM images of an OS-TSPM with green color after calcining: curved (h) and flat surface (i) of the OS-TSPM under bright field (reflection mode); curved surface (j) and flat surface (k) of the OS-TSPM under dark field (reflection mode); (*l*) the OS-TSPM (transmission mode). m) Reflection spectra of the OS-TSPM before and after calcining. n–s) Scanning electron microscopy (SEM) images of OS-TSPMs (after calcining): (n–q) curved and (r–s) flat surfaces of the OS-TSPMs.

etching).[20] Furthermore, during purification and redispersion, the IO-TSPM's polymer hydrogel skeleton absorbed a substantial quantity of water, expanding in size from ~1443 to ~1765 μm (Figure 2g). The lattice spacing *d* would rise ~22.3% as a result (assuming a uniformly crosslinked hydrogel network). The wavelength shift brought on by the decrease in refractive index was partially countered but not entirely compensated for by the hydrogel's swelling, which increased the lattice spacing. The photonic phenomenon underwent a blue shift as a result of the combined effects of reduced refractive index and increased lattice spacing. The transition from SiO_2 CPs-based O-TSPMs to hydrogels-based IO-TSPMs (also shown in Figure S15 (Supporting Information) for blue and red IO-TSPMs) exhibits a similar pattern.[21] The TS of the freeze-dried TSPM was preserved under the SEM analysis (Figure S16, Supporting Information).

Given that the skeleton of the IO-TSPMs was negatively charged polymers pAAm-co-AAc, which can react with positively charged compositions, such as positively charged linear polymers. Ruthenium-functionalized linear polymers, i.e., pNIPAAm-co-Ru(bpy)$_3$ have been intensively studied due to their multiresponsive properties, including thermo-, photoresponsive, and fluorescence properties.[22] The IO-TSPMs can be modified with the pNIPAAm-co-Ru(bpy)$_3$ polymers simply by immersing and electrostatically interacting with the IO-TSPMs in an aqueous solution of the linear polymers (Figures S17–S19, Supporting Information). The IO-TSPM exhibited

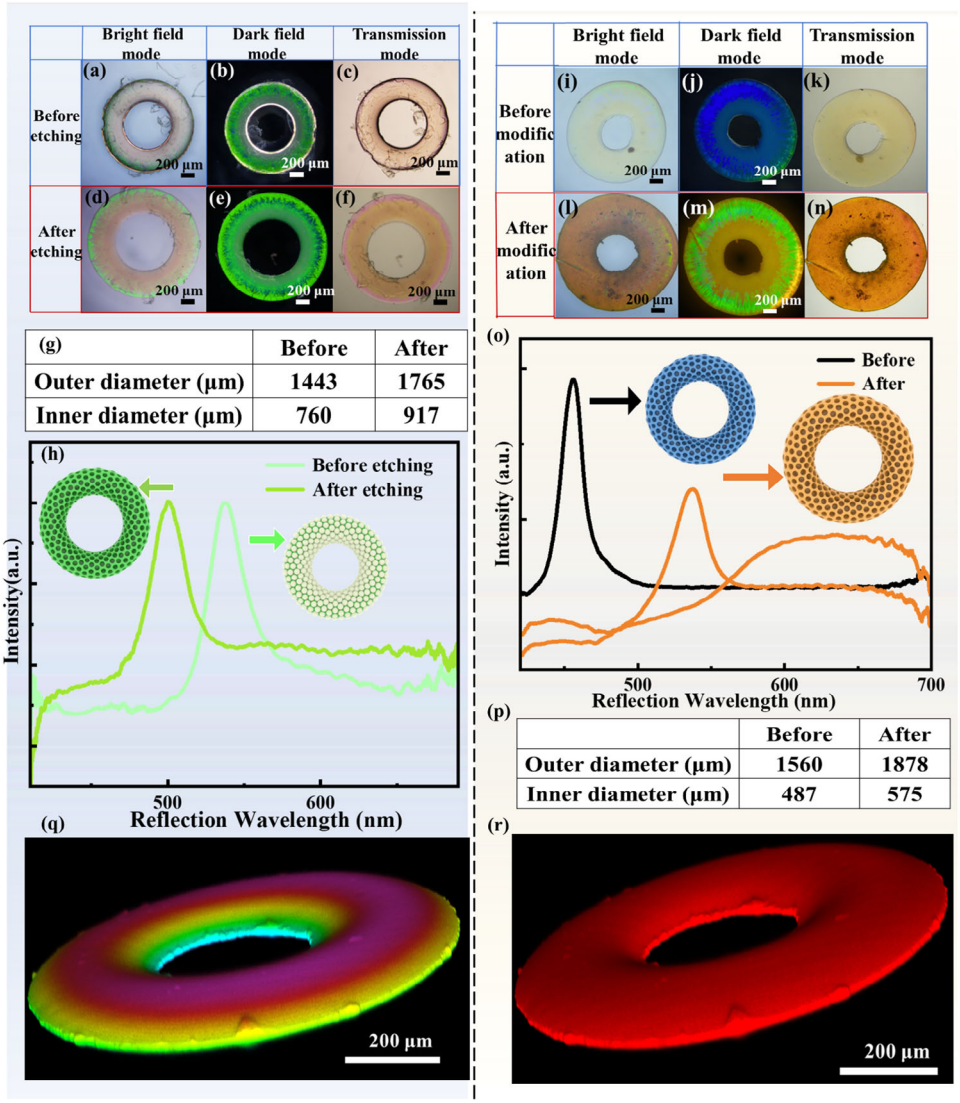

Figure 2. a–c) OM images of green SiO_2 CPs-hydrogel C-TSPM before etching under:(a) Bright field reflection mode. (b) Dark field reflection mode. (c) Transmission mode. d–f) OM images of the IO-TSPM after etching under: (d) bright field reflection mode. (e) dark field reflection mode. (f) Transmission mode. g) Diameter of the green TSPM before and after etching. h) Reflectance spectra of the green TSPM before and after etching. i–k) OM images of an IO-TSPM before labeling with the pNIPAAm-co-Ru(bpy)$_3$ polymers under: bright field reflection mode(i). Reflection mode under dark field (j). Transmission mode (k). l–n) OM images of IO-TSPM after labeling with the pNIPAAm-co-Ru(bpy)$_3$ polymers under: bright (l) and dark(m) fields of reflection mode. Transmission mode (n). o) Reflection spectra of the TSPM before and after labeling with the pNIPAAm-co-Ru(bpy)$_3$ polymers. p) Diameter of the IO-TSPM before and after labeling with the pNIPAAm-co-Ru(bpy)$_3$ polymers. q,r) 3D projection confocal image of an IO-TSPM functionalized with the pNIPAAm-co-Ru(bpy)$_3$ polymers.

different phenomena under reflection mode before and after labeling with the ruthenium-based polymer. The IO-TSPM with the initial blue hue (Figure 2i,j) switched to green and even orange after labeling (Figure 2l,m). The MLCT effect causes the ruthenium-functionalized linear polymers to appear orange hue in water.[23] Consequently, the resulting IO-TSPMs were decorated with an orange hue when viewed under the optical microscope (Figure 2n). Visual inspection revealed that the entire photonic microobject was orange. These phenomena showed that the structural color of the IO-TSPM shifted toward red after complexing with the polymers, and the IO-TSPM further confirmed this color shift (Figure 2o), with the peak of the reflection spectrum shifting from 455 nm (black curve in Figure 2o) to 537 nm. Additionally, a broad orange peak between 562 and 690 nm appeared after the labeling (orange curve in Figure 2o). The orange color was most likely attributed to the reflection peak from the ruthenium-functionalized linear polymer. Given that the IO-TSPM's outer diameter increased from 1560 to 1878 μm following the ruthenium-polymer labeling (Figure 2p), which should result in at least a ≈20.38% increase in lattice spacing d and consequently a red shift in the structural color. Furthermore, the IO-TSPMs exhibited strong fluorescence due to the incorporation of the ruthenium-functionalized polymers (Figure S20, Supporting Information). 3D reconstruction of the IO-TSPM in Figure 2q,r

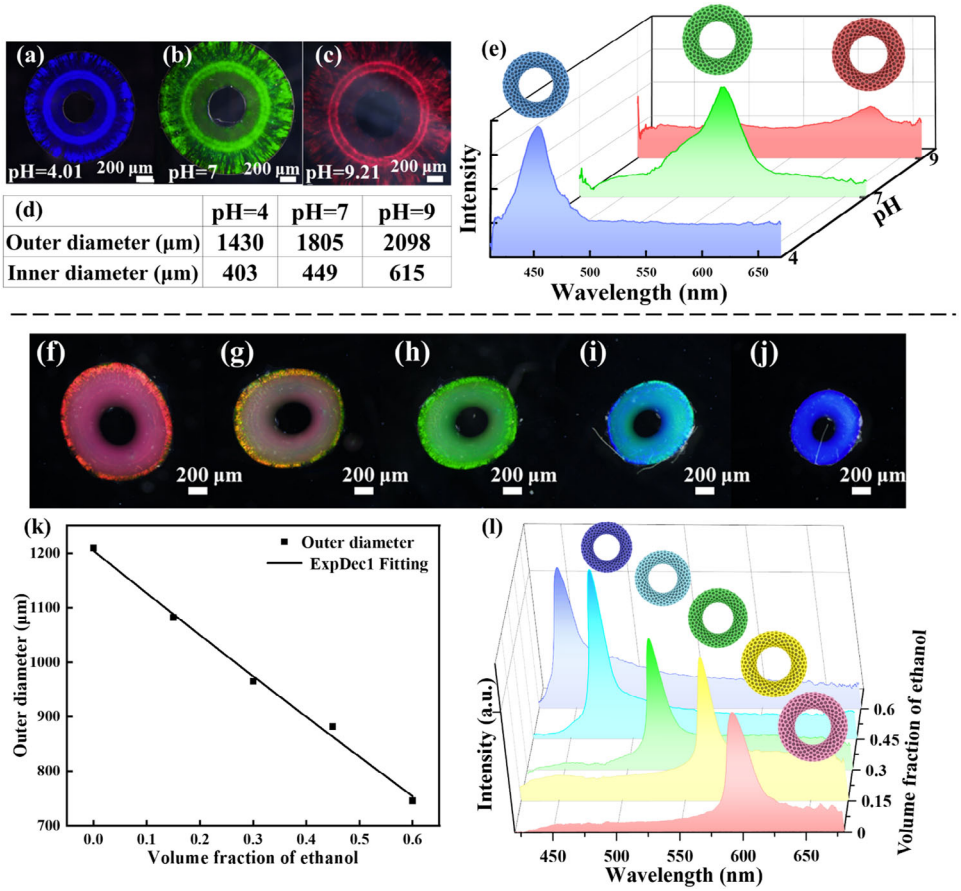

Figure 3. Response behavior to solutions with different pH values: a–c) OM images of the IO-TSPM in solutions with different pH values (a. pH = 4.01 ± 0.02; b. pH = 7.00 ± 0.02; c. pH = 9.21 ± 0.02). d,e) Changes in the outer diameter and reflection spectra of an IO-TSPM in solutions of different pH values. Response behavior to different concentrations of alcohol solutions: f–j) OM images of an IO-TSPM in alcohol solutions of varied concentrations (v/v) (from 0% to 60% (f–j)). k,l) Changes in the outer diameter and reflection spectra of the IO-TSPM in different concentrations of alcohol solutions.

made the microobject with the curved top section even more visible.

For many applications, photonic structures with stimulus-responsive qualities are widely desired.[12a] Hydrogels based on pAAm are renowned for being elastic.[24] By altering the pH levels of the external solutions, the lattice parameters of the photonic microobjects can be tuned to control the swelling or deswelling behaviors of the IO-TSPMs due to the presence of pendant carboxyl groups within the hydrogel skeleton. An IO-TSPM progressively inflated as the pH value increased after being submerged in aqueous solutions with varying pH values. The microobject gradually swelled with pH value increase. The structural colors changed from blue to red at the same time due to this swelling (**Figure** 3a–c). As the pH rose from 4.01 to 9.27, the IO-TSPM's outer diameter expanded from 1430 to 2098 μm (Figure 3d), suggesting a ~46.71% rise in the lattice spacing *d*. The corresponding reflectance peak shifted from 450 to 622 nm (Figure 3e; Figure S21, Supporting Information). From the standpoint of the pKa values, this behavior can be explained. The carboxyl groups on the hydrogel were prone to deprotonate and produce carboxylates when the pH of an external solution exceeded the pKa of pAAc, which was reported to be 4.5.[25] Because of the increased repulsive interaction between the —COO^- groups, the hydrogel skeleton became negatively charged, resulting in considerable swelling. Furthermore, the concentration of ions within the gel increased as a result of the increased charges, changing the osmotic pressure difference between the hydrogel's interior and exterior.[26] Additionally, the osmotic pressure differential may cause the IO-TSPM to inflate, enlarging the macropores and causing a red shift in the reflection spectra according to Bragg's law, and vice versa (Figure S22, Supporting Information).

For photonic microobjects, the reaction to various stimuli is crucial. Various stimulus-responsive characteristics could be used to create analytics platforms with several uses. Here, it has also been investigated how alcohol solutions affect the IO-TSPM's performance. Following immersion in water solutions containing varying alcohol concentrations, the hydrogel-based TSPM de-swelled. Figure 3f–j displayed the microobject's changes both in size and optical phenomena. The size of the IO-TSPM shrank as the amount of alcohol in the aqueous solution grew from 0 to 60 vol%. For instance, the TSPM″s outer diameter of dropped from 1209 to 746 μm (Figure 3k), resulting in a ~38.30% drop in the lattice spacing d and a change in hue from red to purple. As a result, the wavelength of the reflection spectrum changed from 602 to 447 nm (Figure 3l; Figure S23, Supporting Information). The reflectance peak underwent a striking

blue shift (155 nm), resulting in a complete visible color shift from pink to blue. Furthermore, a quick response rate(finished in ~5 s) was guaranteed in the presence of organized macropores, whose diameters were greater than 100 nm (Figure S22, Supporting Information), and allowed for the quick exchange of ions and small molecules across the hydrogel. After several rounds of alcohol stimulus tests, the IO-TSPM's wavelength swiftly recovered to its starting point. Further evidence that the highly ordered 3D porous structure was maintained throughout the multiple cycles of alcohol stimulus-recovery tests came from the IO-TSPM, which showed no discernible optical quality degradation or decrease in the intensity of the reflectance peak during multiple cycles of alcohol concentration changes.

According to several reports, TS microparticles have a shorter diffusion pathway than microspheres.[13,27] But from a visual perspective, no reports have ever supported this assertion. In this respect, we illustrated here how the photonic microobjects' morphologies influenced their stimulus-responsive characteristics. The same batch of droplet templates and the same aqueous solution of monomers were used to create IO-PMSs and IO-TSPMs for the subsequent production of the polymer skeleton construction (as illustrated in Figures S24 and S25, Supporting Information). Stimulus-responsive behaviors were examined from two perspectives in order to determine the two photonic microobjects with distinct geometries: alcohol causes the hydrated photonic microobjects to deswell, while rehydration causes the dehydrated photonic microobjects to swell. At first, both photonic microobjects displayed a red hue in DI water.

The IO-PMS and IO-TSPM were subjected to identical conditions for air-drying (≈5 min) and producing dehydrated gel samples in order to validate the performance benefits of the TS structure. The IO-PMS has a deformed shape because the original IO-PMS was more susceptible to deformation during the dehydration process than the IO-TSPM.[27] Subsequently, these dried gel samples were then concurrently submerged in DI water, and a microscope was used to document the structural alterations of the two samples as they underwent water absorption and expansion. The development of dehydrated IO-TSPM and IO-PMS as upon concurrent exposure to DI water was depicted in **Figure** 4a. At first, the dehydration caused both samples to appear blue. Both samples spontaneously started to absorb water and displayed a recovery in shape after being exposed to DI water. This resulted in a progressive redshift because of the gradually increased lattice spacing. But compared to the IO-PMS, the IO-TSPM showed a faster rate of recovery. A distinct behavior was discovered by employing the IO-TSPM's structural color shift, as seen in Figure 4b. The IO-TSPM's inner and outer surfaces changed color simultaneously, suggesting that water molecules might flow into the gel structure in both directions, accelerating absorption and expansion. In addition to increasing the sample's overall expansion speed, this bidirectional diffusion made sure that the expansion process was uniform. Water molecules could only slowly permeate from the outer surface toward the interior of the spherical sample, as seen by the change that was initially restricted to the outer surface. A slower diffusion process and a higher chance of producing concentration gradients and localized inhomogeneities during diffusion were caused by the spherical structure's strikingly different inner and outer surface areas. The IO-TSPM sample's water absorption and diffusion took ~70 s, however, the IO-PMS sample took ~230 s, which is more than three times longer than the IO-TSPM sample (as shown in Figure 4c; another repeat experiment was also displayed in Figure S26, Supporting Information). The suggested various diffusion-induced expansion mechanisms are depicted in Figure 4d,e. According to the results, the IO-TSPM outperformed the spherical counterpart in terms of response speed. As shown in Figure 4d, the IO-TSPM specifically demonstrated a faster response time during both bidirectional expansion and shrinkage, successfully maximizing and managing diffusion processes. Faster diffusion rates and the avoidance of localized material accumulation were made possible by the IO-TSPM's effective bidirectional diffusion between its inner and outer surfaces. Localized concentration imbalances may result from the reduced overall diffusion efficiency of microspheres limited by unidirectional diffusion (Figure 4e).

On the other hand, a behavior that responded to a reversal stimulation was also confirmed. A hydrated IO-TSPM and a hydrated IO-PMS were first transferred into pure alcohol to accomplish this validation. The evolution behavior of an IO-TSPM in the solution was displayed in **Figure** 5a. In contrast, Figure 5b,c (also shown in Figure S27 and Video S1, Supporting Information) illustrated when an IO-PMS and another hydrated IO-TSPM were placed together, the IO-TSPM finished deswelling in ~90 s, whereas the IO-PMS took over 150 s to reach deswelling equilibrium. According to the findings, the IO-TSPM's shrinkage rate was also noticeably quicker than the IO-PMS. Two different diffusion-induced deswelling mechanisms were suggested, as shown in Figure 5d,e. Alcohol was able to diffuse from both its inner and exterior surfaces toward the interior for the IO-TSPM, which sped up the deswelling and reaction. The IO-PMS limited by unidirectional diffusion, on the other hand, can only diffuse from their outer surface, in which causes an abnormally long deswelling period.

Overall, due to their distinctive geometric shape, we have shown for the first time visually that the hydrogel-based TS microparticles can offer a more effective material exchange, which could result in improved reaction control during diffusion processes. By taking use of the special geometry, the TS design facilitates improved contact and possibly higher reaction efficiency. Higher diffusion efficiency is made possible by this special geometry, especially in procedures that call for quick reactions and sensitive material distribution. In particular, because of the TS's bidirectional diffusion properties, the TS microparticles perform noticeably better than the spherical ones in situations when quick and consistent expansion or shrinking is needed. Comparably, TS structures highlight their wide range of prospective applications in payload delivery systems, catalyst support, and chemical reactors.

3. Conclusion

In summary, we have effectively created IO-TSPMs based on the stimulus-responsive hydrogel. We showed that TSPMs are superior to spherical ones in terms of responsive rate. This was laccomplished by preparing monodisperse SiO_2 CPs as the building blocks for uniform OS-TSPMs. Following collection, a methodical investigation was conducted into the development of the droplets on various surfaces and their ultimate superstructures.

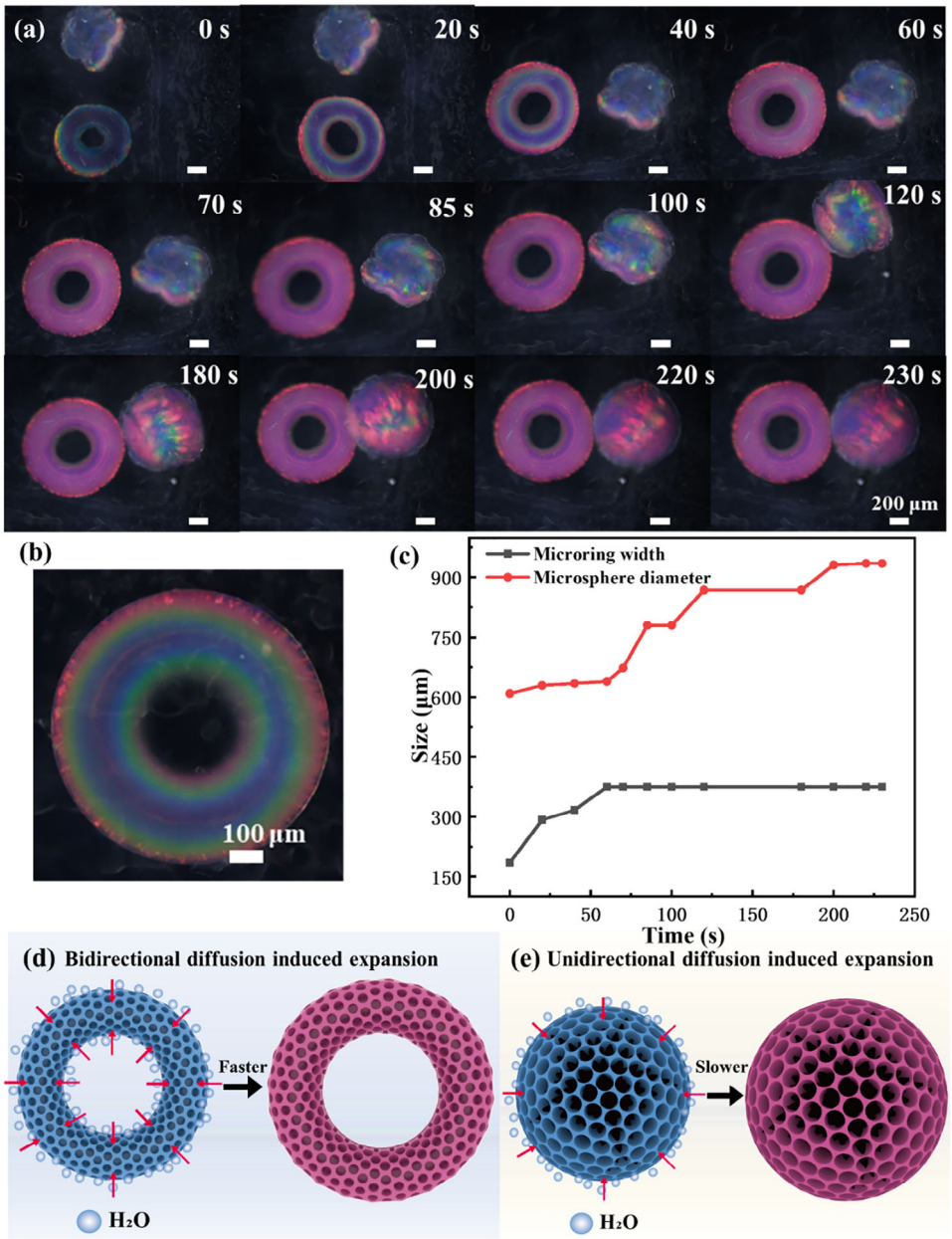

Figure 4. a) OM images of an IO-TSPM and an IO-PMS that were both initially under dehydrated state and expanded with time after being exposed to DI water. b) OM images of the expansion of IO-TSPM induced by the bidirectional diffusion mechanism after exposure to water. c) Diameter changes with time during the expansion of the IO-TSPM and the IO-PMS. d) Schematic diagram of the bidirectional diffusion-induced expansion of an IO-TSPM. e) Schematic diagram of the unidirectional diffusion-induced expansion of an IO-PMS.

The OS-TSPMs were then transformed into IO-TSPMs by using the pAAm-co-AAc based hydrogel as the matrix material. Because of the inherent characteristics of the polymer hydrogel, the resultant IO-TSPMs demonstrated reversible, stimuli-responsive characteristics to alcohol and pH changes. Furthermore, the positively charged linear polymers pNIPAAm-co-Ru(bpy)$_3$ were electrostatically decorated onto the IO-TSPMs to give them a variety of features, including photonic stopbands, fluorescence capabilities, and distinct hues from the ruthenium component. More significantly, we have demonstrated that IO-TSPMs respond more quickly than IO-PMSs. This advantage results from the distinct diffusion mechanisms: IO-TSPMs exhibit bidirectional diffusion of small molecules, whereas IO-PMSs exhibit unidirectional diffusion. We think that this finding might be applied to a range of other materials and inspire researchers to create novel structures for a variety of uses. This finding in particular provides a valuable guide for the design of innovative payload delivery vehicles and sensing devices, which are anticipated to find additional use in the sectors of bioengineering, sensing, and medicine.

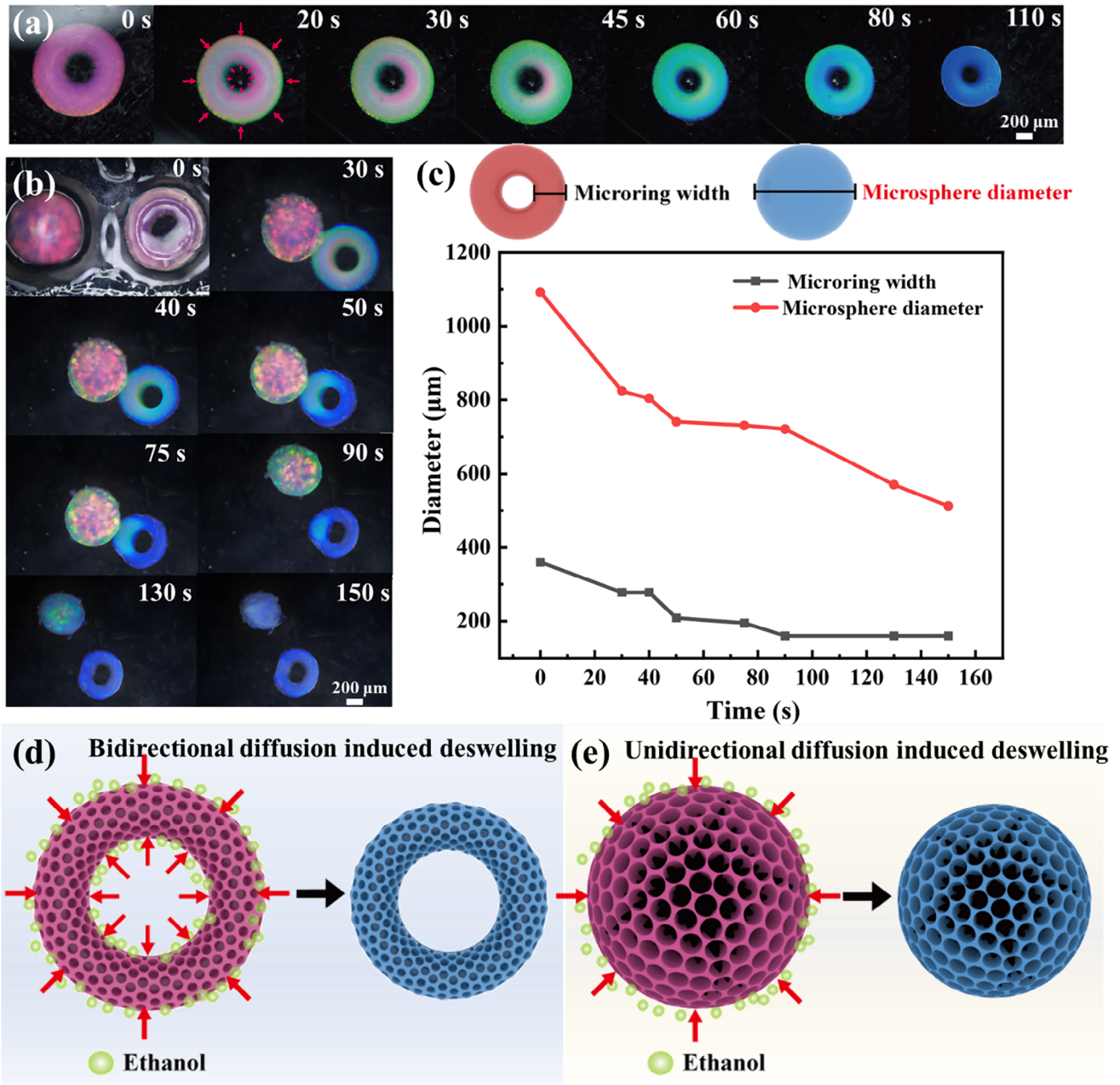

Figure 5. a) OM images show the bidirectional diffusion-induced shrinkage behavior of an IO-TSPM after exposure to alcohol. b) OM images of the shrinkage behaviors of a hydrated IO-TSPM (not the same IO-TSPM as in Figure 5a) and IO-PMS after exposure to alcohol. c) Size changes as a function of time for the two samples in b. d) A schematic diagram shows the bidirectional diffusion-induced deswelling of the IO-TSPM in b. e) The schematic diagram represents the unidirectional diffusion-induced deswelling of the IO-PMS in b.

Supporting Information

Supporting Information is available from the Wiley Online Library or from the author.

Acknowledgements

This work was supported by the Fundamental Research Funds for the Central Universities (No. 2023JBMC021 (Y H.), V24ZYCX00020(X.D.)). Y.H. is also grateful for the open research funds support from Guangdong Provincial Key Laboratory of Technique and Equipment for Macromolecular Advanced Manufacturing (No. 20240518), the fund from Hubei Provincial Key Laboratory of Green Materials for Light Industry, Hubei University of Technology, and Fund of Key Laboratory of Advanced Materials of Ministry of Education (Tsinghua University) No. Advmat-2402. The authors are grateful to Dr. Xinghao Yan from Tsinghua University for his assistance with the confocal imaging. Mr. (Dr.) Fu Wang from Beijing Jiaotong University with his support for the TEM characterizations is also acknowledged.

Conflict of Interest

The authors declare no conflict of interest.

Data Availability Statement

The data that support the findings of this study are available from the corresponding author upon reasonable request.

Keywords

bidirectionally propagate, inverse opal, photonic microobjects, stimulus-responsive, torus-shaped

Received: December 12, 2024
Revised: March 18, 2025
Published online: April 16, 2025

[1] a) M. Liu, J. Fu, S. Yang, Y. Wang, L. Jin, S. H. Nah, Y. Gao, Y. Ning, C. B. Murray, S. Yang, *Adv. Mater.* **2023**, *35*, 2207985; b) Y. G. Kim, S. Park, S. H. Kim, *ACS Nano* **2023**, *17*, 2782; c) A. Hensley, T. E. Videbaek, H. Seyforth, W. M. Jacobs, W. B. Rogers, *Nat. Commun.* **2023**, *14*, 4237; d) J. Zhang, Y. Qin, Y. Ou, Y. Shen, B. Tang, X. Zhang, Z. Yu, *Angew. Chem., Int. Ed.* **2022**, *61*, 202206339; e) Z. Cai, Z. Li, S. Ravaine, M. He, Y. Song, Y. Yin, H. Zheng, J. Teng, A. Zhang, *Chem. Soc. Rev.* **2021**, *50*, 5898.

[2] a) T. Kanai, D. Lee, H. C. Shum, R. K. Shah, D. A. Weitz, *Adv. Mater.* **2010**, *22*, 4998; b) K. Zhou, T. Tian, C. Wang, H. W. Zhao, N. Gao, H. Yin, P. Wang, B. J. Ravoo, G. T. Li, *J. Am. Chem. Soc.* **2020**, *142*, 20605; c) Z. Wang, R. T. Li, Y. T. Zhang, C. L. C. Chan, J. S. Haataja, K. Yu, R. M. Parker, S. Vignolini, *Adv. Mater.* **2023**, *35*, 2207923; d) J. Wang, H. Le-The, Z. Wang, H. Li, M. Jin, A. van den Berg, G. Zhou, L. I. Segerink, L. Shui, J. C. T. Eijkel, *ACS Nano* **2019**, *13*, 3638; e) J. Wang, C. F. Mbah, T. Przybilla, B. Apeleo Zubiri, E. Spiecker, M. Engel, N. Vogel, *Nat. Commun.* **2018**, *9*, 5259.

[3] a) Q. He, H. Vijayamohanan, J. Li, T. M. Swager, *J. Am. Chem. Soc.* **2022**, *144*, 5661; b) J. Lee, S. Ban, K. Jo, H. S. Oh, J. Cho, K. H. Ku, *ACS Nano* **2024**, *18*, 5196.

[4] a) J. Teyssier, S. V. Saenko, D. van der Marel, M. C. Milinkovitch, *Nat. Commun.* **2015**, *6*, 6368; b) J. Xue, X. Yin, L. Xue, C. Zhang, S. Dong, L. Yang, Y. Fang, Y. Li, L. Li, J. Cui, *Nat. Commun.* **2022**, *13*, 7823.

[5] K. Xu, J.-h. Xu, Y.-c. Lu, G.-S. Luo, *Crystal* **2014**, *14*, 401.

[6] a) S. N. Yin, S. Yang, C. F. Wang, S. Chen, *J. Am. Chem. Soc.* **2016**, *138*, 566; b) H. Wang, Y. Liu, Z. Chen, L. Sun, Y. Zhao, *Sci. Adv.* **2020**, *6*, aay1438.

[7] a) O. D. Velev, A. M. Lenhoff, E. W. Kaler, *Science* **2000**, *287*, 2240; b) V. Rastogi, S. Melle, O. G. Calderón, A. A. García, M. Marquez, O. D. Velev, *Adv. Mater.* **2008**, *20*, 4263.

[8] Z. Lu, A. Rezk, F. Jativa, L. Yeo, X. Zhang, *Nanoscale* **2017**, *9*, 13441.

[9] M. Sperling, M. Gradzielski, *Gels* **2017**, *3*, 15.

[10] I. Karimipour, Y. Tadi Beni, H. Arvin, A. H. Akbarzadeh, *Thin-Walled Struct.* **2021**, *165*, 107995.

[11] a) H. Kawaguchi, K. Umesato, K. Takahashi, K. Yamane, R. Morita, K.-i. Yuyama, S. Kawano, K. Miyamoto, M. Kohri, T. Omatsu, *Nanophotonics* **2022**, *11*, 855; b) M. B. Bigdeli, P. A. Tsai, *Langmuir* **2020**, *36*, 4835.

[12] a) Y. Wu, Y. Wang, S. Zhang, S. Wu, *ACS Nano* **2021**, *15*, 15720; b) W. Zhang, H. Tian, T. Liu, H. Liu, F. Zhao, X. Li, C. Wang, X. Chen, J. Shao, *Mater. Horiz.* **2023**, *10*, 2024; c) M. Vatankhah-Varnosfaderani, A. N. Keith, Y. Cong, H. Liang, M. Rosenthal, M. Sztucki, C. Clair, S. Magonov, D. A. Ivanov, A. V. Dobrynin, S. S. Sheiko, *Science* **2018**, *359*, 1509.

[13] D. An, A. Warning, K. G. Yancey, C.-T. Chang, V. R. Kern, A. K. Datta, P. H. Steen, D. Luo, M. Ma, *Nat. Commun.* **2016**, *7*, 12401.

[14] R. D. Deegan, O. Bakajin, T. F. Dupont, G. Huber, S. R. Nagel, T. A. Witten, *Nature* **1997**, *389*, 827.

[15] a) S. Lee, M. T. A., G. Cho, J. Lee, *Nanomaterials* **2022**, *12*, 2600; b) J. Zhou, J. Yang, Z. Gu, G. Zhang, Y. Wei, X. Yao, Y. Song, L. Jiang, *ACS Appl. Mater. Interfaces* **2015**, *7*, 22644.

[16] W. Li, C. Zhang, Y. Wang, *Adv. Colloid Interface Sci.* **2024**, 103286.

[17] T. Nisisako, T. Torii, T. Takahashi, Y. Takizawa, *Adv. Mater.* **2006**, *18*, 1152.

[18] K. E. Torrance, E. M. Sparrow, *J. Opt. Soc. Am.* **1967**, *57*, 1105.

[19] H. Takagi, R. Maeda, T. R. Chung, T. Suga, *Sens. Actuators A:phys.* **1998**, *70*, 164.

[20] G. Wu, L. Yang, H. Qi, D. Li, W. Wei, X. Zhang, *Optik* **2018**, *155*, 171.

[21] W. Li, N. Gao, W. Zhang, K. Feng, K. Zhou, H. Zhao, G. He, W. Liu, G. Li, *Nanoscale* **2023**, *15*, 9339.

[22] D. Suzuki, T. Sakai, R. Yoshida, *Angew. Chem., Int. Ed.* **2008**, *47*, 917.

[23] J.-L. Fillaut, *Coord. Chem. Rev.* **2024**, *518*, 216050.

[24] G. Sennakesavan, M. Mostakhdemin, L. K. Dkhar, A. Seyfoddin, S. J. Fatihhi, *Polym. Degrad. Stab.* **2020**, *180*, 109308.

[25] a) M. Wiśniewska, T. Urban, E. Grządka, V. I. Zarko, V. M. Gun'ko, *Colloid. Polym. Sci.* **2014**, *292*, 699; b) K. K. Das, P. Somasundaran, *Colloids Surf. A Physicochem. Eng. Asp.* **2001**, *182*, 25.

[26] a) S. Migliozzi, G. Meridiano, P. Angeli, L. Mazzei, *Soft Matter* **2020**, *16*, 9799; b) L. S. Lim, N. A. Rosli, I. Ahmad, A. Mat Lazim, M. C. I. Mohd Amin, *Nanomaterials* **2017**, *7*, 399.

[27] S. Ungphaiboon, D. Attia, G. Gomez d'Ayala, P. Sansongsak, F. Cellesi, N. Tirelli, *Soft Matter* **2010**, *6*, 4070.